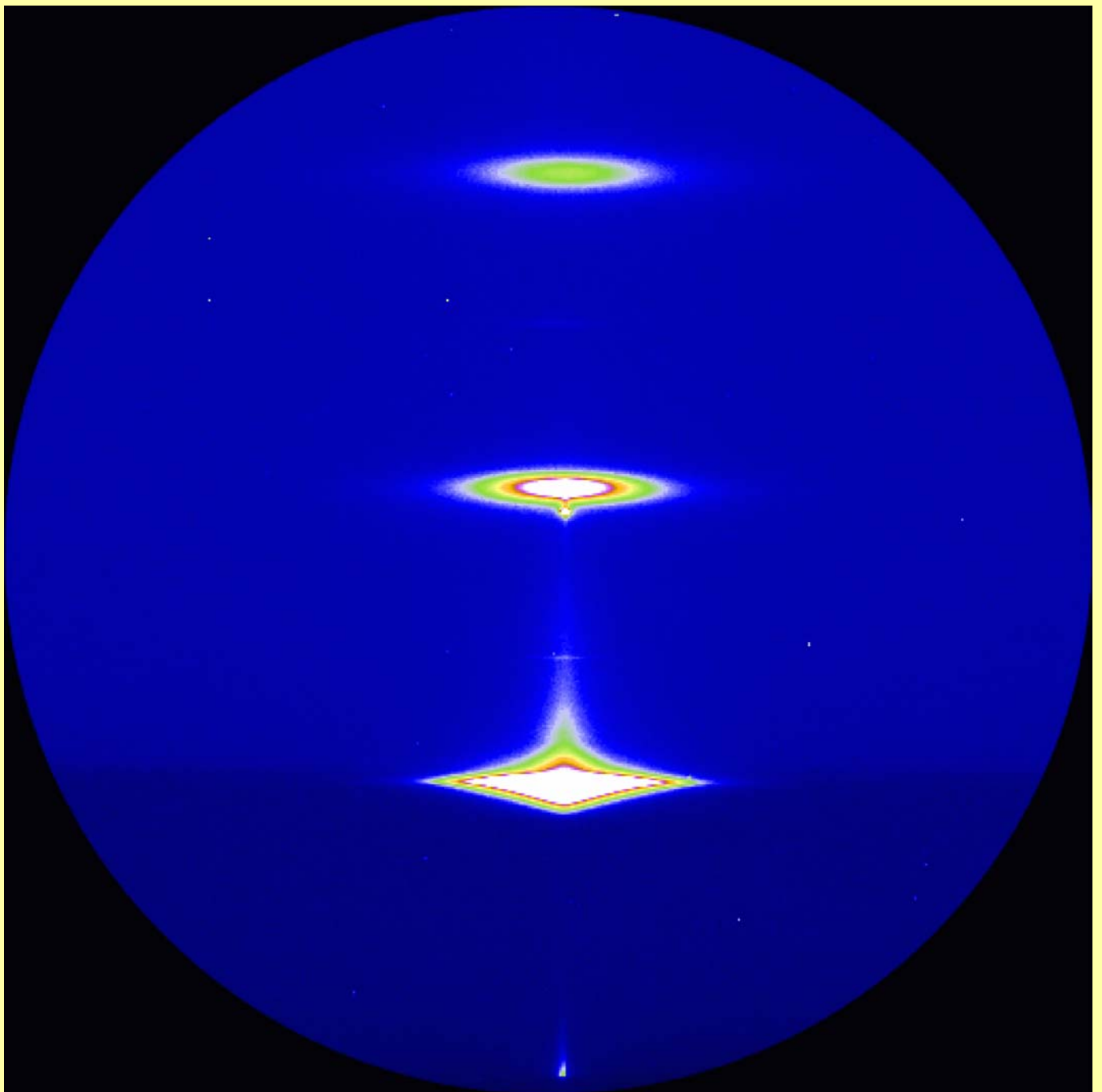




NEWSLETTER

November 2003



Status	2
Instrumental developments	3
Some recent experiments	7
In-house research	12
The XMaS team	13
News round-up	14
Guidelines for applying for beam-time at the XMaS beamline	15

Status

The last 12 months saw the start of our new 5 year grant from EPSRC, which includes several new provisions. For example the beamline on-site team has increased from four to five with the appointment of Laurence Bouchenoire as a third beamline scientist. She is just emerging from the strain of PhD thesis production, having written everything you could possibly want to know about phase plates. The increase in staffing was somewhat negated by Simon Brown's slipped disc(s) which saw him sidelined and supine for the best part of 5 months, a period which also saw the arrival of a baby daughter. Congratulations to Simon and Lol and also to Danny and Dina who married in September 2003.

The new grant contains specific funds for two major items of new equipment. The first is an area detector which is now on the beamline, has been commissioned and is now in regular use. The second equally expensive new facility will be a 4 Tesla superconducting magnet designed to be compatible with diffractometer operation. We are just reaching the end of a design study by American Magnetics, which demonstrates its feasibility. It will have a warm bore and should be able to accommodate most of our sample environments. We hope to have the magnet in place in late Spring 2004.

The 1.7K, three-stage cryostat is now in regular use and can routinely reach that base temperature in all orientations. In a trial experiment reported by Danny Mannix elsewhere in this Newsletter we made one run with ^3He rather than ^4He and broke the 1.0K barrier. We intend to make this available as a user facility.

The *xyz* cryostat mount, along with the tube slits, the in-vacuum slits and the polarisation analyser, are being marketed by Huber who will be only too willing to give you a quote for all of the above!

The Project Management Committee is now under the Chairmanship of Denis Grieg who took over from Ted Forgan. The Peer Review Panel is chaired by Sean Langridge and its ex-chair, Bob Cernik, is now a regular member of the PMC. We are grateful to Denis and Sean for accepting their important new roles and we thank all the other members who have "retired" from their involvement with XMaS. We also welcome our new EPSRC representative Simon Crook, and thank Becky Haskins whom he replaces. The current membership of the PMC and the PRP is given on page 14. We also said goodbye to ESRF's CRG liaison officer, Ian Kilvington and welcome his successor, Axel Kaprolat.

Cover illustration: Image from the new beamline MAR ccd camera of low angle diffuse x-ray scatter from a 60-period Co/Ru multilayer. The lower scatter streak, extended in the sample plane, arises at the critical angle. The upper two scatter streaks occur at the second and third Bragg sheets and result from conformal roughness. A small spot of specular scatter is visible below the Bragg sheet.

Studies at 1.0 Kelvin on XMaS Resonant X-ray Magnetic Scattering on TmNi₂B₂C

D. Mannix, P. B. Thompson, S. Pujol, X. Tonon—for further information contact D. Mannix at XMaS, BM28, ESRF. danny@esrf.fr

XMaS has in routine use a prototype adaptation of a closed cycle refrigerator system developed by the cryogenics group at the ILL. A continuous flow of ⁴He gas, forced through a Joule-Thompson jet, provides the additional cooling at the dispex tail that reduces the sample environment base temperature from the 10K of the standard dispex down to 1.7K. The system can be used in both vertical and horizontal scattering geometries and can be combined with a number of other experimental techniques, for example, with azimuthal scans and also with the XMaS 1.0 Tesla electromagnet.

Recently, an experiment was performed with ³He replacing the ⁴He flowing through the Joule-Thompson jet. A base temperature of 1.0K was achieved in a resonant x-ray magnetic scattering (RXMS) experiment to investigate the spin density wave (SDW) antiferromagnetism formed in TmNi₂B₂C. TmNi₂B₂C is a celebrated compound because of the co-existence of superconductivity (T_c=11K) and magnetism (T_N=1.5K) at low temperatures. The (1±τ 1±τ 10) spin density wave satellites, at T=1K, together with the (1 1 10) Bragg intensity are shown in Figure 1. Polarisation analysis was used to measure the σπ component of the scattered intensity (i.e. the component of the incident σ photons scattered with a π-phase shift).

Dipole RXMS scatters photons uniquely with this polarisation, whereas the presence of the central (110) Bragg peak in the π channel arises only through ‘cross-

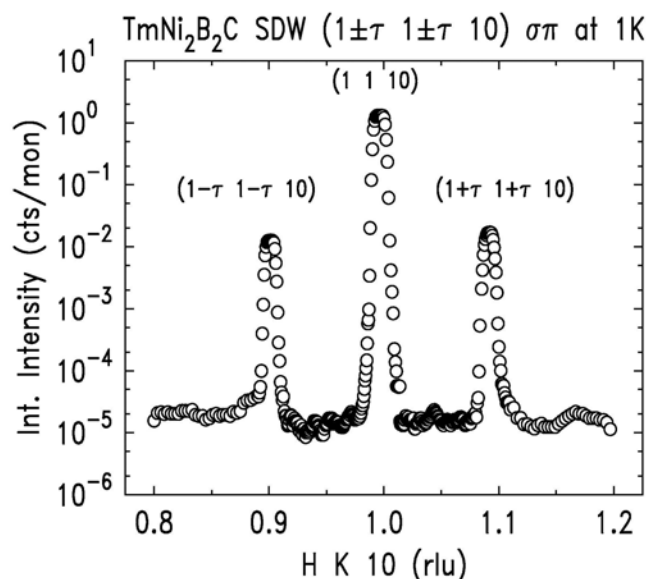


Figure 1 The (1±τ 1±τ 10) SDW satellites and central (1 1 10) Bragg peak of TmNi₂B₂C at 1.0K.

talk’ (σπ leakage through the analyser). Figure 2 shows the temperature dependence of the (1+τ 1+τ 10) SDW together with data from neutron scattering. Very good agreement is found between the thermal evolution of the magnetic sublattice and T_N for both scattering techniques.

It was found necessary, during the acquisition of the RXMS data, to attenuate the beam by two orders of magnitude to avoid excessive local heating of the sample by the intense x-ray beam. Future measurements are planned using an exchange gas to try to reduce this effect.

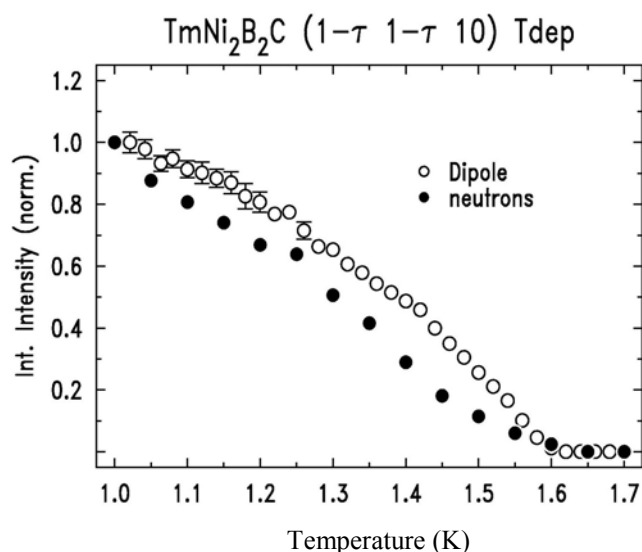


Figure 2. The temperature dependence of the (1+τ 1+τ 10) SDW RXMS satellite intensities (open circles) compared with published neutron data (filled circles)

Commissioning studies with the MAR CCD area detector

C. A. Lucas, P. B. Thompson — for further information contact P. B. Thompson at XMaS, BM28, ESRF. pthompo@esrf.fr

A MAR CCD area detector has been delivered and recently commissioned through the medium of some preliminary test experiments. One of the experiments was a continuation study of the structure and reaction kinetics at an electrode surface in an electrochemical cell by x-ray scattering. Since the detector allows the possibility of time-dependent studies, the growth of a Cu film on a Au substrate was examined from “snap shot” diffraction images of the surface over an electrodeposition/dissolution cycle. With the novel cell design, incorporating close temperature control, it is possible to influence the mobility of solution species in the electrolyte that, in turn, changes the kinetics of surface chemical reactions and phase transitions.

Figure 2 shows two images of scattering measured at reciprocal lattice position $(0,0,3.385)$ in the conventional hexagonal reciprocal lattice notation used for the Au(111) surface. At this reciprocal lattice point there is scattering from the Au surface observed prior to Cu deposition (upper panel). After deposition of Cu the scattering changes dramatically as this is the reciprocal space position where diffraction from Cu(111) planes also occurs. The spot profile becomes extended in the horizontal plane consistent with diffuse scattering from the Cu deposit. These two images represent the two end points (clean surface and Cu film deposited) of a complete data set which was taken with a 10 second time resolution both during the growth of the Cu film and then its dissolution. Similar measurements at other key reciprocal lattice points will help to build a detailed picture of the mechanism of Cu electrodeposition.

Such experiments can easily be extended to other systems, for example, real time studies of catalytic reactions and ordering phenomena at electrochemical and biological interfaces are planned in the near future.

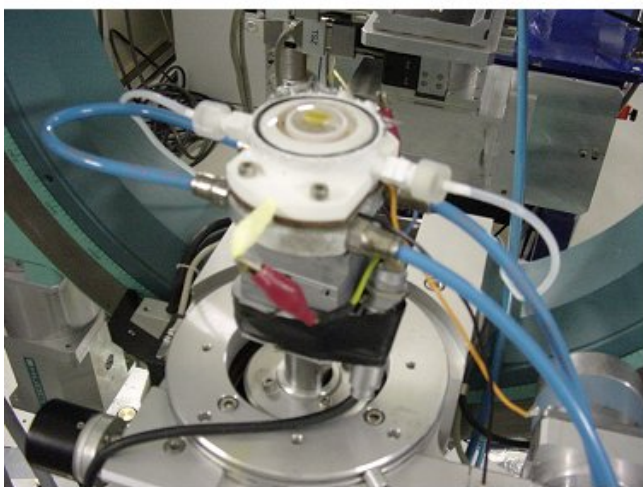


Figure 1 The variable-temperature electrochemical cell mounted on the XMaS diffractometer

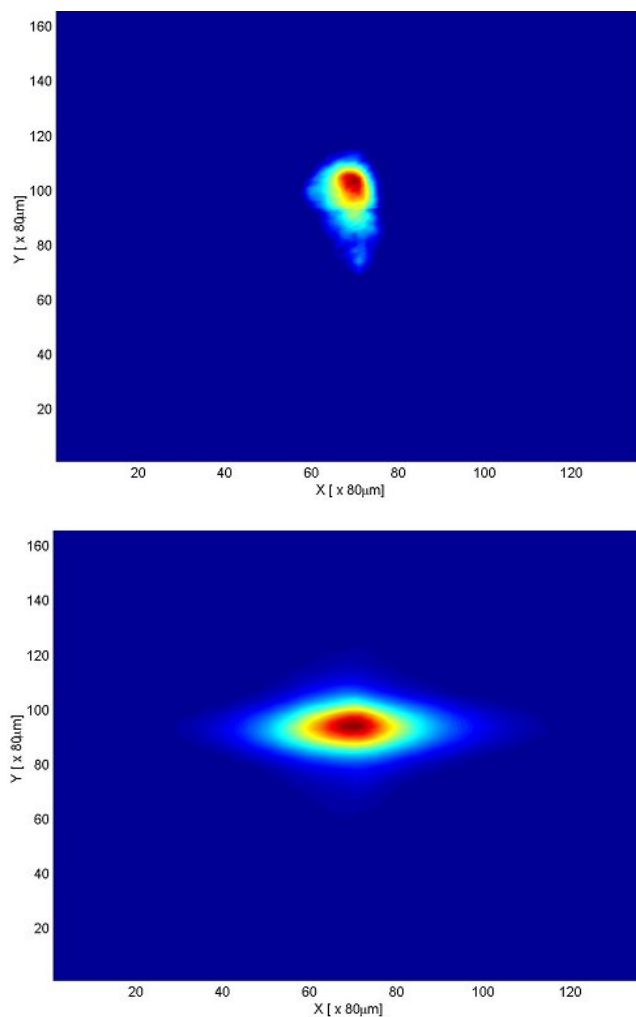


Figure 2 Images of scattering at the reciprocal lattice position $(0,0,3.385)$ - (upper) prior to Cu deposition on the Au surface, (lower) after Cu deposition.

Maximising flux

Efforts continue to reduce attenuation losses caused by air paths and vacuum closing screens. To this end a number of developments have been completed including a new in-vacuum slit assembly for use on the diffractometer 2theta arm, shown in Figure 1. The maximum opening aperture of this screen, formed from four tungsten blades, is 12mm x 12 mm. Each jaw can be independently positioned to within $2\mu\text{m}$ and all axes have limit switches to prevent mechanical damage. A cyberstar detector has been acquired, also for use on the 2θ arm, with a vacuum flange adaptation that allows integration of the detector into the same vacuum path—saving 2 capton windows and an air gap.

Progress has been made upstream of and, in some instances, around the sample for certain experimental setups in order to allow the application of a magnetic field at low temperatures and remove entry and exit window absorption from the beam path. An in-vacuum magnet-

cryostat has been designed and made. The main body of the vacuum vessel is supported on the XMaS XYZ mount on the chi circle to allow for precise sample alignment. To ensure efficient cooling, the coil of the electro-magnet is mounted ex-vacuum, below the vacuum vessel. The iron magnet yoke passes through seals in the base of the vacuum vessel. The tips of the adjustable magnet pole pieces, inside the vacuum vessel, support a copper sample stub via three ceramic balls to minimize thermal losses. An ARS DE202 displacer is mounted on the Huber chi cradle on rubber anti-vibration dampers and intrudes into the vacuum vessel through a bellows. A short copper braid connects the sample stub to the tip of the second stage of the cryostat. The incident and outgoing beam paths consist of two large mechanically supported bellows, whose terminations communicate with the upstream and diffractometer-2 θ -arm vacuum paths. The maximum scattering angle allowed within the constraints of the bellows is 30 degrees in theta and 60 degrees in 2 θ . Figure 2 shows a schematic of this experimental setup.

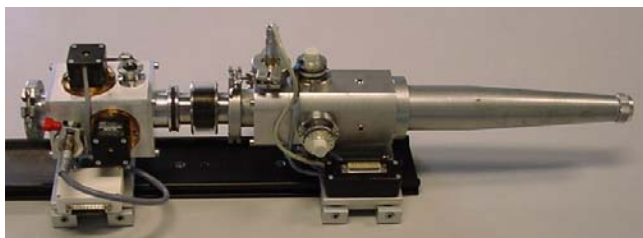


Figure 1 shows the XMaS in-vacuum slit system and illustrates how it can be “vacuum integrated” with the “tube slits” to form a beam collimator.

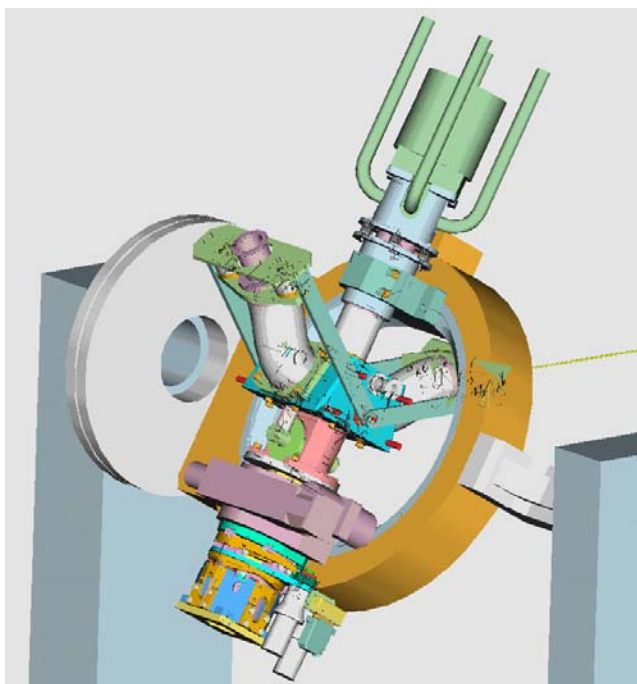


Figure 2 shows an evacuated sample environment that incorporates a magnet and sample cooling from a displacer that is mechanically isolated from the sample.

A 100 mm thick diamond has been purchased to produce circularly polarized x-rays for low energy experiments. It has been commissioned in an experiment with the energy

set at the uranium M₄ edge, 3728 eV. At this energy, it transmits 20% of the photons in contrast to only 1% for the 300 mm thick diamond in our possession. Integration of the phase plate into the vacuum, shown in Figure 3, leads to a further gain of 2 orders of magnitude in flux at these energies, i.e. more than 10³ flux gain overall.

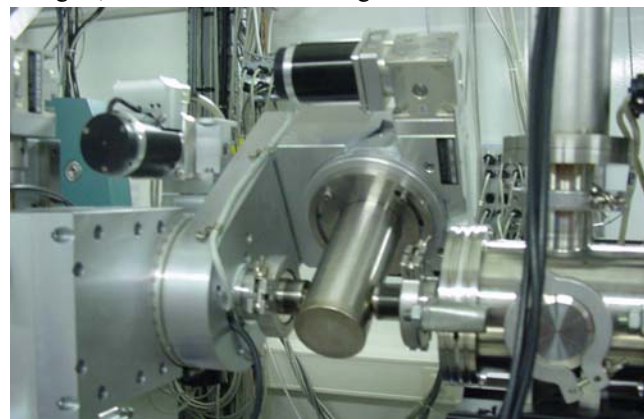


Figure 3 In this view the phase plate assembly is enclosed in a vacuum shroud with bellows continuing the beam and vacuum paths upstream and downstream.

Channelcut polariser for magnetic diffraction

Phase-plates are used generally for experiments that require a maximum degree of circular polarisation (e.g. XMCD, reflectivity). For diffraction experiments however, the approach is rather different because the magnetic signal is proportional to the factor of polarisation, $f_p = P_C / (1 - P_l)$ where P_l and P_C are the degree of linear and circular polarisation of the beam, respectively. This implies that the magnetic effect is maximised when the value of P_l is very close to unity, and hence when P_C is small. It has been observed frequently that the flipping ratios measured during diffraction experiments using either the inclined view method or a phase-plate, were swamped by beam movements. This is because P_C varies every time the orbit moves and then f_p changes significantly.

A Si (333) channelcut polariser was inserted upstream of the phase-plate to minimise this effect. A test experiment was performed at 8.65 keV an energy chosen so that the channelcut crystal was set at a Bragg angle close to 45° thereby producing an exit beam that was almost completely linearly polarised. Source movements now produce intensity rather than polarisation fluctuations in the exit beam. The 0.3 mm thick diamond phase-plate was then used to condition the beam before it was scattered horizontally at 90° from an iron (110) single crystal. Figure 1 shows the variation of the f_p as a function of $\Delta\theta$, the angular offset of the diamond from the Bragg condition. The data were obtained for a beam size of 1x10 mm² (blue triangles) and 1x50 mm² (red squares) and by reversing the magnetisation of the sample. The theoretical curves were calculated for P_l equal to 99.996% (yellow line) and 99.994% (green line) for the beam incident on the phase plate. The models fit extremely well at negative $\Delta\theta$: the discrepancies at positive $\Delta\theta$ are attributed to the presence of a multiple reflection in the diamond.

The channelcut polariser improves the value of f_p by an order of magnitude but, more importantly, it effectively removes the polarisation fluctuations arising from source movement which were previously preventing measurements being made. In this method it will also be possible to reverse the helicity keeping the magnetic field constant, thereby extending the scope of the technique to harder magnetic materials.

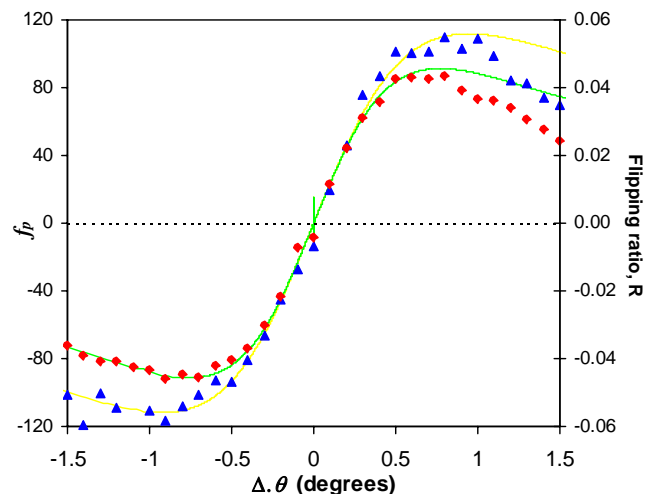


Figure 1 Experimental polarisation factor, f_p , at Ψ equal to 43° as a function of $\Delta\theta$ obtained for a beam of $1 \times 10 \text{ mm}^2$ (blue triangles) and $1 \times 50 \text{ mm}^2$ (red squares) at 8.65 keV. The theoretical curves were calculated for P_i equal to 99.996% (yellow line) and 99.994% (green line).

The 4 Tesla magnet

We commissioned American Magnetics Inc. to perform a design study, in collaboration with the XMaS team, for a superconducting split coil magnet system that can be mounted on the beamline Huber diffractometer and deliver a field of 4 T in a large 40 mm opening warm bore. The proposed design functions without the use of liquid helium enabling diffraction in a number of geometries. A high strength mid plane spacer is needed to support the 55,000 N force generated across the 180 degree diffraction slot.

The magnet, supported from the base of the diffractometer, has been designed to fit within the Eulerian cradle to allow several versatile field orientations as shown in Figures 1-3. Thus vertical, transverse and longitudinal field orientations are possible. The efficient yoke configuration occupies a little less than half of the scattering plane, allowing 180 of angular access for the cryostat and scattered beam.

Our standard and low-temperature adapted displaces have too large a section to fit within a 40 mm bore and so a new, small-section two-stage displax, capable of reaching 10K in its standard configuration, is to be purchased and will have a third stage adaptation added to enable it to operate down to 1.7° K using ^4He and 1°K with ^3He over a wide range of angles without degradation of the cooling performance.

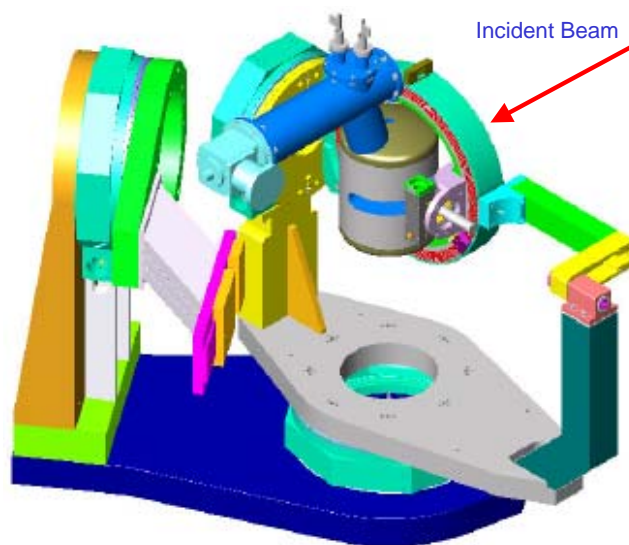


Figure 1.4 Tesla vertical field horizontal scattering

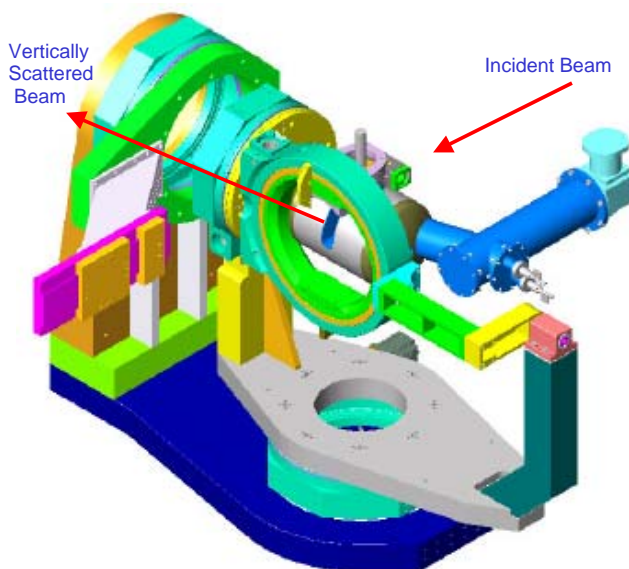


Figure 2 4 Tesla transverse field for vertical scattering and horizontal scattering— $\pm 5^\circ$

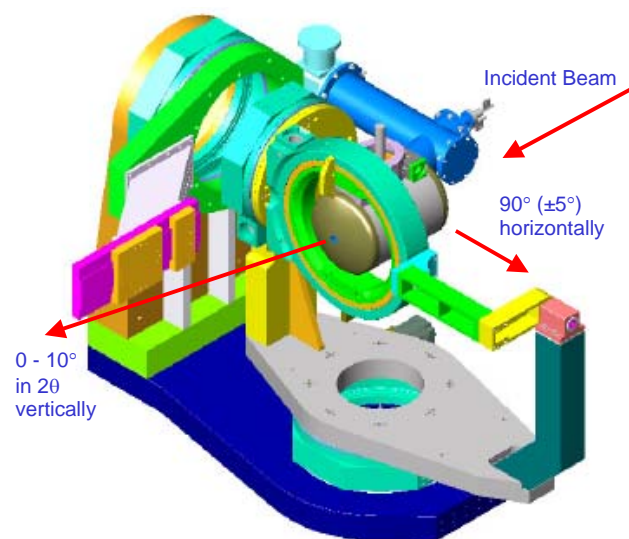


Figure 3 4 Tesla longitudinal field (parallel to x-ray beam) for $90^\circ \pm 5^\circ$ horizontal scattering— $\pm 5^\circ$ and $0-10^\circ$ in 2θ vertically

Thermal motion induced scattering from zinc oxide

S. P. Collins, D. Laundy, V. E. Dmitrienko, D. Mannix, P. Thompson - for further information contact S. P. Collins at Daresbury Laboratory, Warrington, WA4 4AD, U.K. (S.P.Collins@dl.ac.uk)

The effect of temperature on the intensity of x-ray diffraction has been understood since the subject was in its infancy. Perturbing the positions of atoms, through thermal vibrations, normally leads to a reduced scattering strength. However, Dmitrienko *et al* recently predicted that, under certain conditions, the reverse would be true: increasing temperature would actually increase the diffraction intensities. The requirements for observing such an effect are quite stringent. The reflection must be one that is forbidden by the normal space-group extinction rules, even after accounting for dipolar anisotropy in the (resonant) scattering amplitude, and the photon energy must be close to an absorption edge. However, the reflection must be allowed for a scattering response that transforms as a third rank tensor, since Templeton and Templeton predicted this to be the lowest order tensor to describe any physical phenomena of this symmetry.

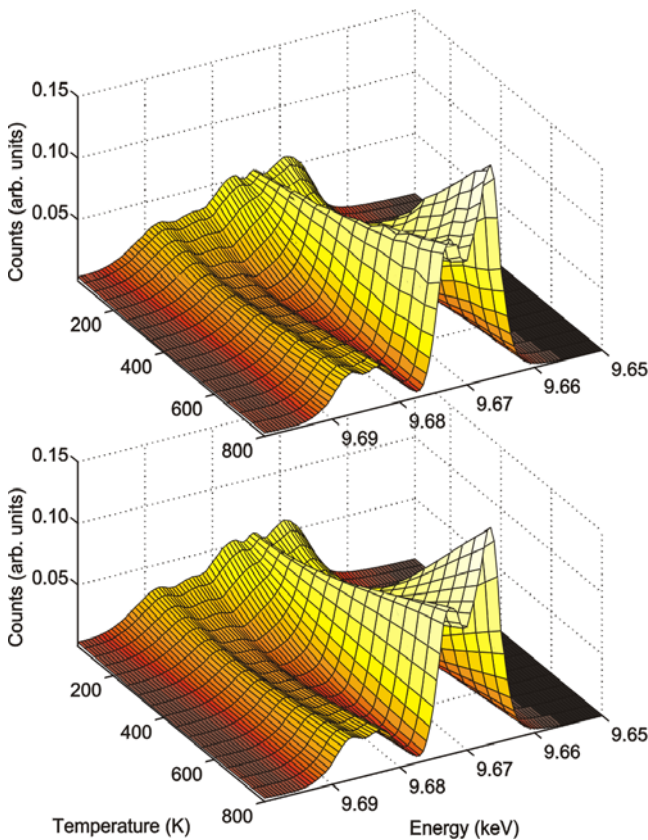


Figure 1 ZnO 115 absorption-corrected resonant intensity versus energy and temperature. Top: measured intensities; Bottom: intensities from a least-squares fit to a phenomenological model, based on two competing resonance processes.

Previously, a number of observations of this effect have been made in germanium, where the energy spectrum of the ‘forbidden’ reflections was found to be essentially single resonance. In the present work, we have measured thermal-motion-induced (TMI) scattering in hexagonal ZnO (space group $P6_3mc$) on the XMaS beamline, and found, for the first time, the complex and strongly temperature dependent resonance spectrum shown in Figure 1. The complexity arises because there are two competing scattering processes: mixed dipole-quadrupole (E1E2) resonances, and TMI scattering. By using a simple phenomenological model, whereby the E1E2 amplitude is constant while the TMI part increases rapidly with temperature, we have been able to reproduce the data very precisely, and extract the amplitudes and relative phases of the two components.

Both of these processes are of fundamental interest in x-ray physics. The E1E2 signal is directly sensitive to hybridization in the valence state, while the TMI scattering gives a unique insight into the evolution of electronic structure with nuclear position.

Anomalous Coupling of Spin and Lattice Degrees of Freedom in GdB_6

D.F. McMorrow, K.A. McEwen, J.G. Park and S. Lee—for further information contact K. A. McEwen at Dept. of Physics & Astronomy, University College, London, WC1E 6BT (K.mcewen@ucl.ac.uk)

Rare-earth hexaboride compounds crystallise in the cubic CaB_6 structure, see Figure 1, and display a wide variety of magnetic phenomena. Examples include CeB_6 , a prototypical heavy-Fermion Kondo lattice system, for which open questions still remain concerning the nature of the order parameter, and SmB_6 which is an archetypal Kondo insulator.

For GdB_6 , the Gd^{3+} ions are in an s state ($L=0, J=S=7/2$) and consequently it might be expected that this compound should display properties associated with a simple, spin-only, Heisenberg magnet. This turns out not to be the case. At high temperatures the susceptibility follows the Curie-Weiss law, with $S=7/2$ and a paramagnetic Curie temperature of 60 K. With decreasing temperature the susceptibility begins to deviate from Curie-Weiss behaviour, and around 30 K a Schottky anomaly appears in the specific heat. It has been suggested that these anomalies in the paramagnetic phase arise from short-range magnetic correlations due to the frustrating effect of next-nearest-neighbour and next-next-nearest-neighbour exchange interactions. At lower temperatures still, two magnetic transitions occur at $T_1 \gg 16$ K and $T_2 \gg 10$ K, both believed to be into antiferromagnetic phases.

Using XMaS we have performed a detailed x-ray scattering study of the magnetic and structural properties of GdB₆. Off resonance, satellite peaks appear with modulation wave vectors of $q_1=(0,0,1/2)$ and $q_2=(1/2,1/2,0)$ below T_1 and T_2 respectively, Figure 2. By analysing their polarisation characteristics, and variation with wave vector transfer, we conclude that they arise from a lattice modulation, Figure 3(a) and (b). In an earlier study these satellite peaks had been identified incorrectly as being magnetic in origin. With the photon energy tuned to the L_{II} edge of Gd, a third set of satellite peaks was discovered with $q_3=(1/4,1/4,1/2)$ for temperatures below T_1 , Figure 3 (c) and (d). This was shown to be the true magnetic order parameter. The phase diagram, constructed from detailed measurements of the temperature dependence, polarisation characteristics, and variation with azimuthal angle of the scattering, reveals a surprisingly rich interaction between the spin and lattice degrees of freedom in this compound. A full analysis of the data will reveal the origin of the anomalous coupling between the spin and lattice degrees of freedom in this intriguing compound.

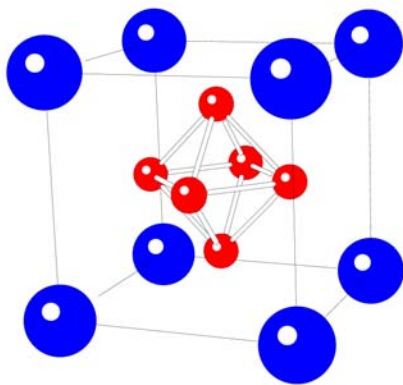


Figure 1 The crystal structure of GdB₆.

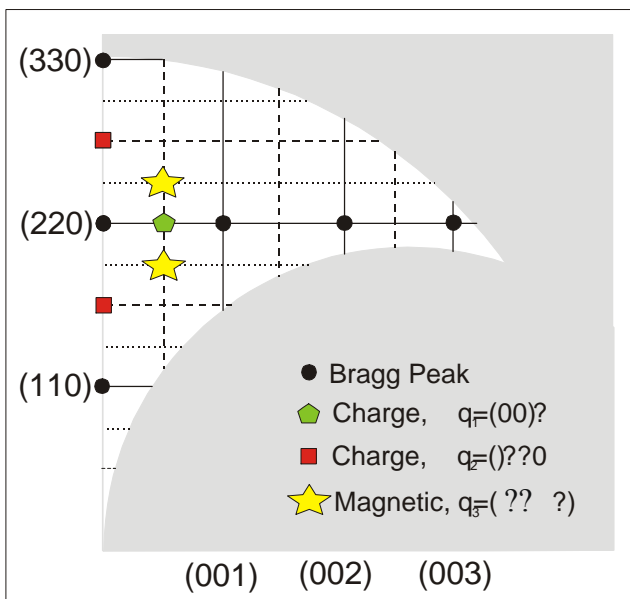


Figure 2 A map of the accessible region of reciprocal space for energies in the vicinity of the L₂ edge of Gd

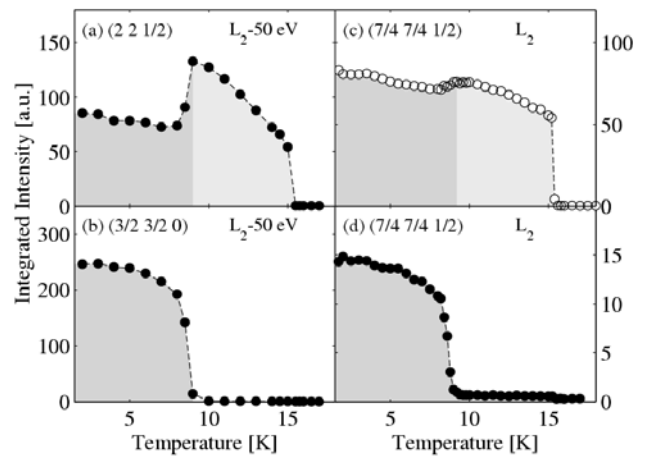


Figure 3 (a)-(b) Temperature dependence of the non-resonant scattering in the $\sigma \rightarrow \sigma$ channel (closed symbols), where two distinct charge satellites are evident with $q_1=(0,0,1/2)$ and $q_2=(1/2,1/2,0)$. (c) At resonance a third peak appears with $q_3=(1/4,1/4,1/2)$. As it occurs in the $\sigma \rightarrow \pi$ channel (open symbols), and displays a sharp resonance at the L₂ edge it is magnetic. (d) At low temperatures q_3 develops a $\sigma \rightarrow \sigma$ component.

Ordering at a free surface, a buried interface and the bulk of a polymer thin film

M Durell, P C Jukes, A Das, D Trolley, M Geoghegan, R A L Jones and J E Macdonald. For further details, contact J E Macdonald at Dept. of Physics & Astronomy, University of Wales, Cardiff macdonald@cf.ac.uk

The central aim of our programme is to determine experimentally the effect of a free surface or buried interface on developing crystalline, long-ranged order in polymer systems. This is an important issue practically because many important macroscopic properties of polymers – particularly thin polymer films - are controlled by their surfaces and interfaces. For example adhesion, friction and barrier properties of a film are expected to be significantly different if the surface of the film is substantially crystalline rather than amorphous. These issues have gained new urgency with the near market development of polymer electronics.

The detailed kinetics can be followed in real-time using a compact high vacuum chamber for in-situ studies: studies to date have focused on poly(ethylene terephthalate) (PET), an archetypal crystalline polymer. Grazing incidence diffraction allows the surface and bulk behaviour to be resolved by varying the angle of incidence of the x-ray beam. A buried polymer interface can also be probed, in principle, by refraction at an interface between a less dense upper layer and a denser lower layer.

A comparison of the bulk and surface crystallisation is shown in Figures 1(a) and (b): the surface crystallizes more rapidly. At annealing temperatures of 85°C and 90°C, the surface crystallizes but not the bulk. Parallel in-situ AFM

studies at Cardiff show the time-evolution of the morphology of the crystalline regions, Figure 2. The crystallisation is also thickness-dependent: the buried interface with the silicon affects both the kinetics and the crystalline morphology for thicknesses below 300 Å. The effect of a buried polymer interface is shown in Figure 3. This shows grazing incidence diffraction from a PET interface with a less dense polystyrene (PS) overlayer. The difference in the critical angle for PET and PS is of the order of 0.02° and hence considerable care was required to penetrate the PS while limiting the penetration in the PET film. The time-resolved scans show that the interfacial PET crystallizes initially at 95°C but the crystallinity is lost after about 3 hours due to interdiffusion with PS.

This constitutes the first *in-situ* surface diffraction study of polymer surfaces and buried interfaces. In parallel with *in-situ* AFM, it provides a unique structural probe of polymer thin films. The new area detector on XMaS will give a 50-fold increase in acquisition rate and provide additional depth information, opening up new material systems. The work is being extended to isotactic polystyrene (another semi-crystalline polymer) and to liquid crystalline semiconducting polyfluorene films, where the surface order is closely related to channel mobility in organic field-effect transistor devices.

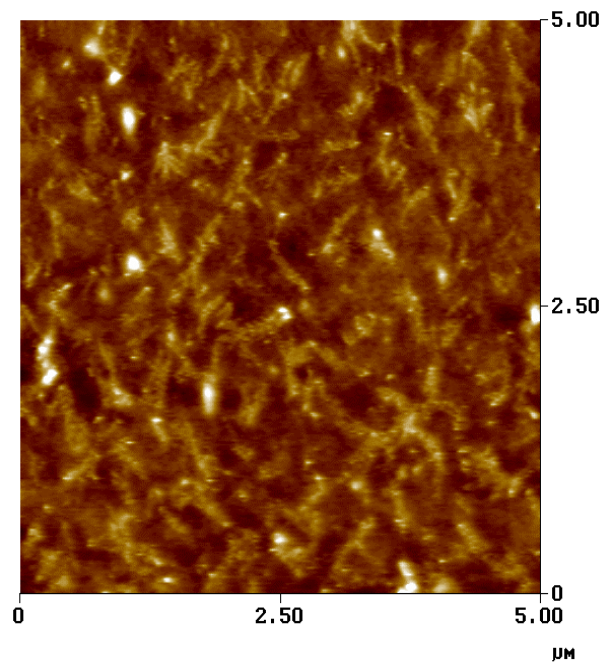
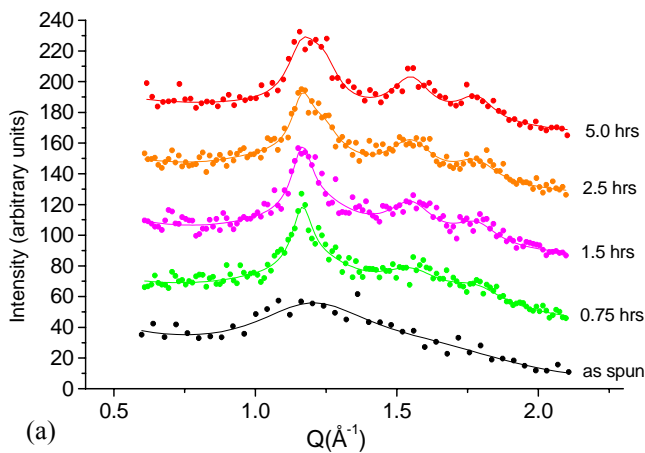
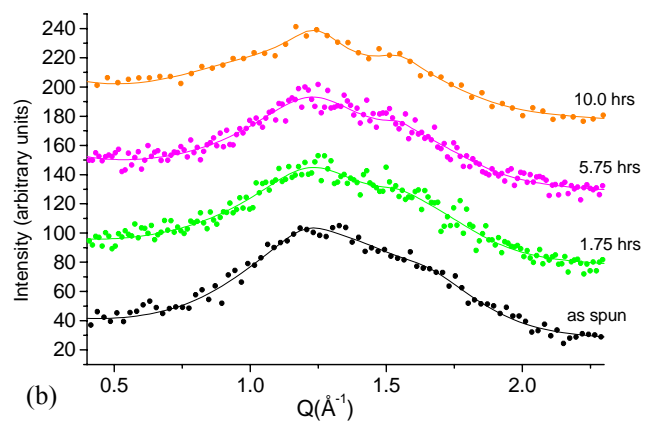


Figure 2 AFM image of PET surface during *in-situ* annealing.



(a)



(b)

Figure 1 (a) bulk and (b) surface grazing incidence diffraction scans for PET during *in-situ* annealing.

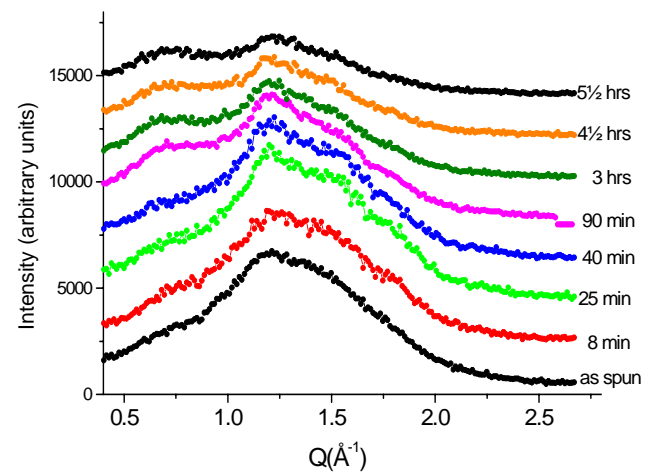


Figure 3 grazing incidence diffraction from interfacial PET at buried interface with polystyrene overlayer.

Effect of epitaxy on the magnetic order of (110) Eu films

S. Soriano, C. Dufour, T. Gouriex, K. Dumesnil and A. Stunault—for further information contact S. Soriano at Laboratoire de Physique des Matériaux, Université H. Poincaré – Nancy 1, BP 239, 54506 Vandoeuvre les Nancy cedex, France. soriano@lpm.u-nancy.fr

The aim of this study was to determine the magnetic phases in single crystal (110) Eu films and to investigate the effect of epitaxy on its magnetic phase diagram. Epitaxial growth may induce strains, clamping effects and symmetry breaking. Bulk europium metal orders at $T_N=90\text{K}$ in a helical phase, with propagation vectors

parallel to the $\langle 100 \rangle$ axes of the bcc structure. Three magnetic domains thus coexist, corresponding to the three helices propagating along the equivalent $\langle 100 \rangle$ directions.

Here we present the temperature dependence of the resonant x-ray magnetic scattering (RXMS) from a 370 nm thick Eu film. As in bulk Eu, at $T_N=90.4\text{K}$ three pairs of magnetic satellites appear simultaneously around the (220) charge peak, see Figure 1. Each pair corresponds to one helix direction, close to a $\langle 100 \rangle$ axis, with the intensity being representative of the domain's population. Cooling below 60 K, the domain population of the helix propagating in the plane of the sample (the [001] domain) shrinks to the benefit of the other two domains. A large hysteresis was observed on re-heating: the domain, with in-plane propagation vector, begins re-populating above 70 K and the equi-populated domain configuration is restored at $\sim 80\text{K}$. Similar behaviour was observed in all films studied. Moreover, the temperature variation of the [001] domain population depends strongly on film thickness, with the two-domains configuration being more stable in the thinner film. In all films, the thermal variation of the turn angle of the helices is very similar for the three magnetic domains and to that measured in bulk europium. However, our RXMS experiments on (110) Eu films have revealed a new intriguing feature compared with bulk behaviour. The out of plane propagation vectors continuously move away from the [100] and [010] crystallographic axes on cooling. In fact, both helix propagation vectors move closer to the perpendicular axis of the sample (i.e. the moments move closer to the sample plane) while the propagation vector located in the sample plane retains its [001] alignment throughout the whole temperature range of existence of the corresponding helix. The value of the tilt angle at a given temperature also depends on the film thickness: it increases when the film thickness decreases and can reach 7° at 10K for a 37nm thick Eu film.

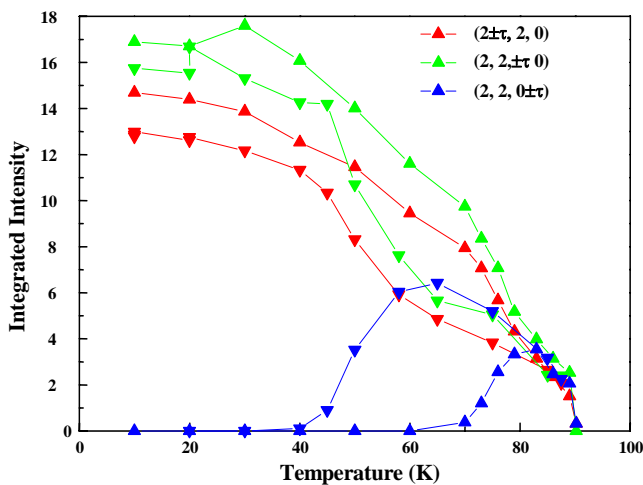


Figure 1 Thermal variation of the integrated intensities (in arbitrary units) of the $(2-\tau, 2, 0)$, $(2, 2-\tau, 0)$ and $(2, 2+\tau, 0+\tau)$ satellites for a 370nm (110) Eu film. Triangles pointing down (up) correspond to data taken on cooling (heating).

The observed preferential population of the two domains is probably due to clamping effects between crystal lattices in the system (substrate, buffer layer, Eu film). A tetragonal lattice distortion is normally associated with the development of helical phases (along the propagation vector). It is assumed that the distortion associated with the in-plane helix produces strains in the sublayers, and thus a significant cost in elastic energy, larger than for the two other helices. The magnetoelastic strains associated with the [001] helix would then be blocked, thus at low temperature a stabilised two-helices configuration becomes energetically more favourable than a distortion of the whole epitaxial system.

Scaling Properties of the Interface Morphology in Fe/Cr Multilayers

T.P.A. Hase, B.K. Tanner, D. F. Paul, L. Bouchenoire—for further information contact T. P. A. Hase at University of

Controversy still surrounds the choice of correlation function used to describe the growth and evolution of interface structure in thin metallic films. The most common correlation function is defined by the interface roughness, the in-plane correlation length, x and h , the fractal or scaling exponent. Due to the cut-off associated with the sample surface, extracting these parameters from the diffuse data measured in the scattering plane is impeded by the limited range of q_x probed. We have measured the scattered intensity out of the scattering plane where there is no such cut-off. Figure 1 shows the intensity as a function of the in-plane momentum transfer, $q_{//}$, defined as:

$$q_{//} = \sqrt{q_x^2 + q_y^2}$$

where q_y is the momentum transfer out of the scattering plane. The data show a power-law decay with an exponent of $\gamma = -3.9 \pm 0.1$. Within a self-similar fractal growth model, this exponent is related to the scaling of the surface through the relation, $\gamma = (2+2h)$, giving a value of the scaling exponent of $h = 0.9 \pm 0.1$. Such a value of h is indicative of sputter deposited systems and similar experiments on MBE systems showed lower values of h , as predicted by growth theories.

The on-set of the scaling was used to estimate the in-plane correlation length as $380 \pm 50\text{\AA}$, consistent with our previous measurements. In deposition, where the kinetic energy of the incident atoms is reduced, a columnar structure can develop and the growth is characterised by the scaling theory for the growth of amorphous films. Here both the in- and out-of-plane correlation lengths, $\xi_{//,x}$, follow the scaling law $\xi_{//,x} \propto q^p$ with p having a characteristic value depending on the statistical nature of the surface. Figure 2 shows the scaling behaviour of the FWHM of the Bragg sheets, which are inversely proportional to ξ . The scaling theory predicts the relation,

$p = (2-h)^{-1}$ for a *self similar surface* and in Figure 2 we see that this is the case for high q_{\parallel} . The UHV deposition of these Fe/Cr samples shows columnar growth with a high degree of conformality between the self-similar interfaces, well modelled by the scaling theory.

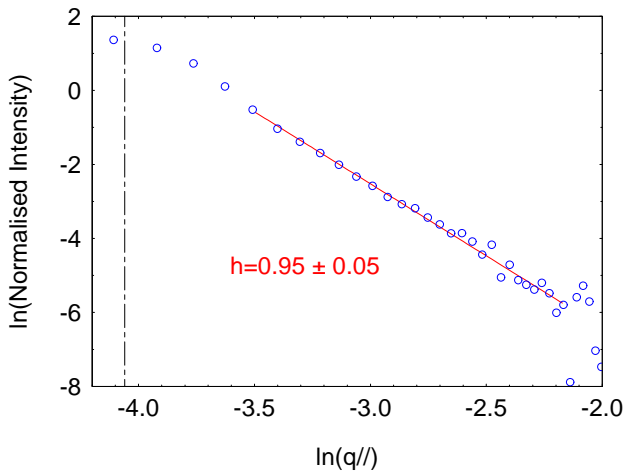


Figure 1: The scaling of the diffuse scatter as a function of in-plane momentum transfer.

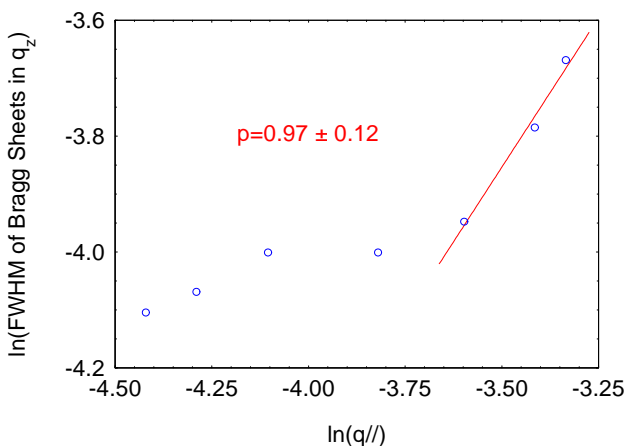


Figure 2: Ln-Ln plot to show the scaling behaviour of the FWHM of the 1st Bragg peak in q_z as a function of q_{\parallel} .

Measurements of coherent scatter profiles for normal and diseased breast tissue

M.J.Farquharson, E.Ryan and K.Geraki—for further information contact M.J.Farquharson, Department of Radiography, Institute of Health Sciences, City University, London, EC1M 6PA m.j.farquharson@city.ac.uk

We want to develop a system that will improve the process of examining biopsy samples thereby improving the diagnosis of breast cancer. The current process is open to interpretive problems and an unequivocal distinction between benign and malignant samples is not always possible.

There is evidence that sufficient differences between benign and malignant tissues exist to make them distinguishable using x-ray scattering. The coherent scattering distribution provides valuable information regarding the molecular structure of the material in question. Materials such as body tissues show oscillatory scattering patterns at small angles, which is characteristic of the short range order and local structure. As each material exhibits a different pattern, it may be used to characterise tissue types. This pilot study aimed to investigate the differences between benign, malignant and healthy (adipose) scatter signatures. These measurements had not previously been performed using a monochromatic synchrotron source or indeed to such a degree of statistical accuracy.

A focussed 12 keV beam (0.5 x 0.5 mm) was incident on the sample. Scatter measurements were made over the range, 5.5° to 50°, with an angular resolution of 0.1°. Further measurements were made at an angular resolution of 0.02° in chosen areas of interest. Beam attenuation was minimised by evacuating the space between the collimating slit assemblies. In this pilot study 12 tissues were examined, 6 malignant tumours and 6 benign, plus 3 adipose.

Corrections have been applied to the data for the different sample thicknesses, the different quantities of tissue within the scattering volume at each angle and the different beam path lengths through each sample. A graph of the averaged corrected data is shown in Figure 1. The results show a significant difference in profile intensity and a slight difference in shape. In order to be able to compare the tissue types properly a detailed knowledge of the tissue composition and density is needed. We are now developing a method for determining the electron density of the tissue. Further measurements are planned with a much larger number of samples.

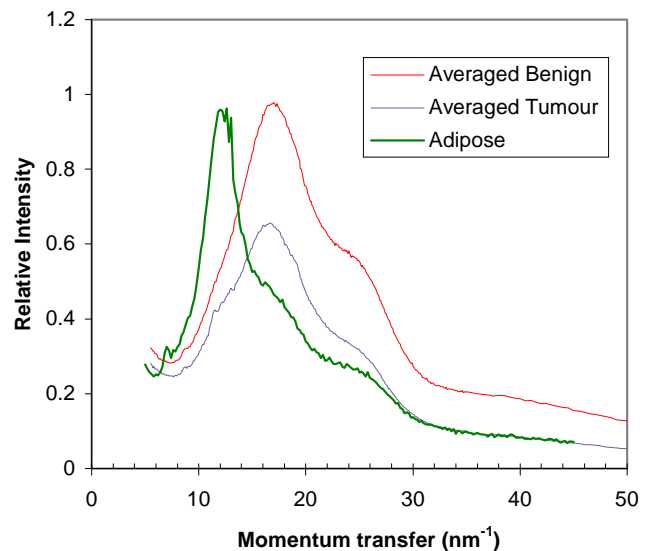


Figure 1. Averaged data for all tissue types

X-ray resonant magnetic scattering from ferromagnetic holmium

*S. D. Brown, L. Bouchenoire, D. Mannix, P. Thompson—
for further information contact S. D. Brown at XMaS,
BM28, ESRF. sbrown@esrf.fr*

X-ray resonant magnetic scattering (XRMS) has been widely employed in the determination of antiferromagnetic structures and studies of magnetic phase transitions. The antiferromagnetic phase of holmium has been studied extensively, elucidating both hitherto unobserved lock-in antiferromagnetic structures as well as two length-scale behaviour of the temperature dependence of T_N . Below 20 K, the helical antiferromagnetic structure transforms to a conical structure, resulting in a c-axis ferromagnetic moment, and the stabilisation of a commensurate $1/6$ c^* modulation wave vector. The precise nature of this transition has proved extremely difficult to determine due to large thermal hysteresis of the antiferromagnetic wave vector.

We have performed the first study of the ferromagnetic phase of holmium using ferromagnetic XRMS. The experiment was performed in a horizontal scattering geometry with the (300) reflection giving a 2θ angle of 95.3° at the holmium L_{III} edge (8.071 keV). A vertical field was applied parallel and anti-parallel to the c-axis to reverse the sign of the charge-magnetic interference scattering. In this geometry, charge, magnetic dipolar and magnetic quadrupolar scattering may all interfere with one-another in the scattered π channel.

The energy dependence of the ferromagnetic scattering at the L_{III} edge is shown in Figure 1. The main peak is dipolar in nature while the lower energy side peak is quadrupolar. Horizontal scattering from the $(0,0,6\pm\tau)$ antiferromagnetic peaks exhibit strong quadrupolar and weak dipolar signals in the uncorrected spectra due to strong ‘white-line’ absorption at the dipolar energy. The data in Fig 1 is not, and does not need to be, corrected for absorption, as the asymmetry ratio is independent of the absolute scattered intensity. The energy dependence of the ferromagnetic scattering at the L_{II} edge is shown in Figure 2. The sign change from positive to negative has been observed in XMCD measurements, but in antiferromagnetic scattering spectra two positive peaks are observed due to insensitivity to the sign of the effect. It is clear that the sensitivity to quadrupolar contributions, the lack of requirement for absorption corrections and the sensitivity to sign changes make this technique well suited to studies of resonant line shapes, which may lead to improved theoretical models.

Changes in magnetic response as a function of focal spot size were observed in the magnetisation curves shown in Figures 3 and 4. With the large spot size, the remanent magnetisation is seen to be only $\sim 30\%$ of the saturated value. With the smaller focal spot size, the remanence approaches the saturated value. Despite efforts to model this behaviour in terms of domain structure, no satisfactory

explanation could be obtained with use of random ‘ising’ type domain structures. One needs to invoke a highly ordered, co-operative reversal mechanism including antiferromagnetically coupled domains to reproduce this behaviour. We could not produce intermediate remanence between the 0.01 and 0.03 values shown in the figure. This behaviour was observed at several different points on the sample. One possible explanation of the probe-size-dependent magnetisation curves is that in increasing the spot size the probe extends beyond the ‘sweet-spot’ of crystallite under investigation. The boundaries between different crystallites might be expected to represent large discontinuities in the local CEF and may couple antiferromagnetically due to the dipole field of the surrounding mosaic blocks. This is, however, pure speculation and more measurements are required to elucidate the true origins of these effects.

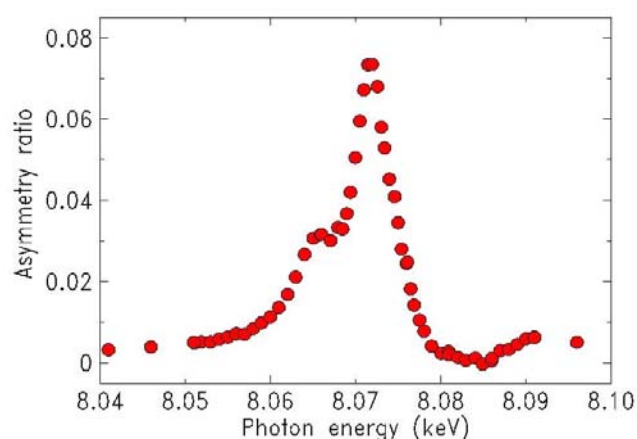


Figure 1 Energy dependence of the asymmetry ratio at the L_{III} edge

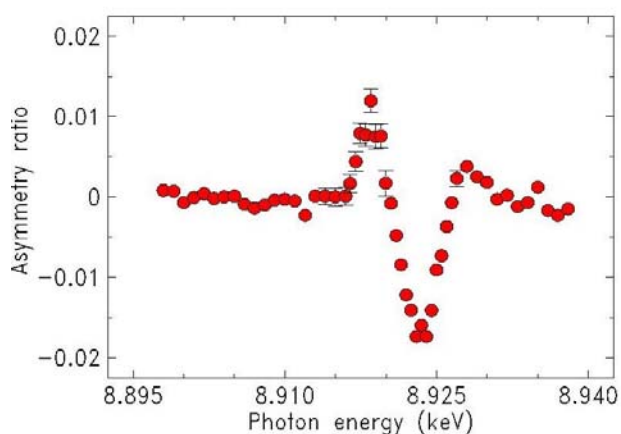


Figure 2 Energy dependence of the asymmetry ratio at the L_{II} edge

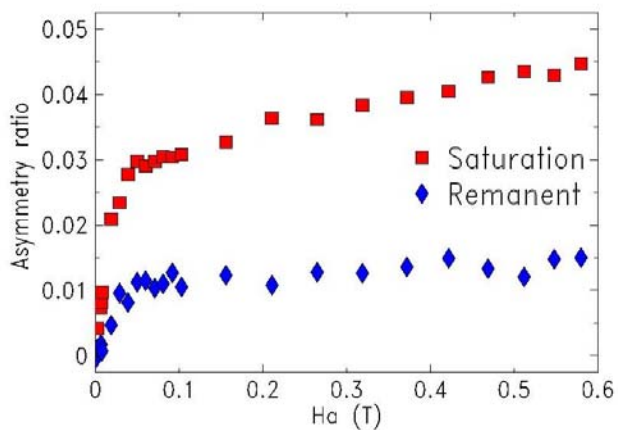


Figure 3 Comparison of saturation and remanent signals as sampled with a 270 x 225 mm² focal spot

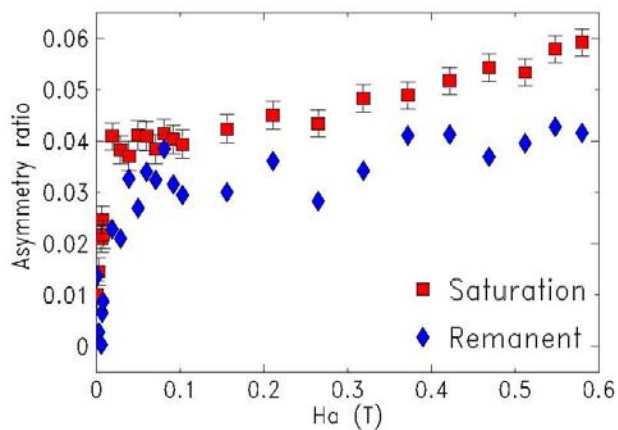


Figure 4 Comparison of saturation and remanent signals as sampled with a 20 x 40 mm² spot

The XMaS Team



Simon



Danny



David



Laurence



Paul

Please note—The experimental reports in the previous pages are all as yet unpublished. Please email the contact person if you are interested in any of them or wish to quote these results elsewhere.

Our web site

This has recently been updated and is at:

http://www.esrf.fr/exp_facilities/BM28/xmas.html

It contains the definitive information about the beamline and an on-line beamline manual.

Living allowances

These are still 55 euros per day per beamline user—the equivalent actually reimbursed in pounds sterling, of course. XMaS will continue to support up to 4 users per experiment if you can make a case for the presence of the fourth experimentalist. The ESRF hostel still appears adequate to accommodate all our users, though CRG users will always have a lower priority than the ESRF's own users. Do remember to complete the web-based “A form” requested of you when you receive the ESRF invitation, all attendees must be listed, since this informs the safety group of the attendees and is used to organise all site passes, meal cards and accommodation.

Beamline people

There has been one change in the beamline staff since the last Newsletter, an additional beamline scientist has been appointed—see under Beamline Scientists below.

Project Co-ordinator - David Paul, (dpaul@esrf.fr), is the person who can provide you with general information about the beamline, application procedures etc. David should normally be your first point of contact.

Beamline Scientists - Simon Brown (sbrown@esrf.fr) and Danny Mannix (danny@esrf.fr) continue as beamline scientists and, since the beginning of December 2002, they have been joined by Laurence Bouchenoire (boucheno@esrf.fr). Laurence, formerly a Warwick University PhD student, was largely based at XMaS where she led the development of our phase plate capability as part of her thesis work.

Technical Support – Paul Thompson (thompso@esrf.fr) continues to work on instrument development and provides technical support for the beamline. John Kervin (jkervin@liv.ac.uk), who is based at Liverpool University, provides further technical back-up and spends part of his time on-site at XMaS.

Malcolm Cooper (m.j.cooper@warwick.ac.uk) and Chris Lucas (clucas@liv.ac.uk) continue to travel between the UK and France to oversee the operation of the beamline. The administration for XMaS continues to be handled by Sandra Beaufoy at Warwick University (s.beaufoy@warwick.ac.uk).

The Project Management Committee

The current membership of the committee is as follows:

Denis Greig (chair)

Des McMorro

Peter Hatton

Jose Baruchel

Bob Cernik

Simon Crook

Meeting twice a year, in addition to the above, the directors, the chair of the PRP and beamline team are in attendance.

The Peer Review Panel

The current membership of the panel is as follows:

Sean Langridge (chair)

Paul Strange

Paul Fewster

Nick Brookes

In addition either Malcolm Cooper or Chris Lucas attend their meetings.

Housekeeping!!

We take some trouble to keep the beamline clean and tidy, please leave the beamline in the same state! At the end of your experiment samples should be removed from cryostat and other sample environment mounts, tools, etc returned to racks and unwanted materials disposed of in an appropriate manner. When travel arrangements are made, therefore, please allow additional time, at the cessation of beam, to effect a tidy-up.

PUBLISH PLEASE!!.....and keep us informed

Although our list of papers reporting work on XMaS is growing we still need more of those publications to appear. We ask you to provide Sandra Beaufoy not only with the reference but also a preprint/reprint for our growing collection. Note that the abstract of a publication can also serve as the experimental report!

IMPORTANT!

When beamline staff have made a significant contribution to your scientific investigation you may naturally want to include them as authors. Otherwise we ask that you add an acknowledgement, of the form:

“This work was performed on the EPSRC-funded XMaS beam line at the ESRF, directed by M.J. Cooper and C.A. Lucas. We are grateful to the beam line team of S.D. Brown, D.F. Paul, D. Mannix, L. Bouchenoire and P. Thompson for their invaluable assistance, and to S. Beaufoy and J. Kervin for additional support.”

Guidelines for Applying for Beam-time at the XMaS beamline

XMaS Pluo B3, ESRF, BP 220, 38043 Grenoble Cedex, France

Tel: +33 (0)4 76 88 24 36 Fax: +33 (0)4 76 88 24 55

web page : http://www.esrf.fr/exp_facilities/BM28/xmas.html

email: dpaul@esrf.fr

Beamline Operation

The XMaS beamline at the ESRF, which came into operation in April 1998, has some 133 days of beam time available each year for UK user experiments, after deducting time allocated for ESRF users, machine dedicated runs and maintenance days. During the year, two long shut-downs of the ESRF are planned: 5 weeks in winter and 4 weeks in summer. At the ESRF beam is available for user experiments 24 hours a day.

Applications for Beam Time

Two proposal review rounds are held each year, with deadlines for submission of applications, normally, the end of **March** and **September** for the scheduling periods August to end of February, and March to July, respectively. **Applications for Beam Time** are to be submitted **electronically** (the paper versions are not acceptable) following the successful model used by the ESRF and ourselves. Please consult the instructions given in the ESRF web page:

www.esrf.fr

Follow the links: “**User Guide**”

And: “**Applying for Beam Time**”

Follow the instructions carefully — you must choose “XMAS-BM28” and “CRG Proposal” at the appropriate stage in the process. A detailed description of the process is always included in the reminder that is emailed to our users shortly before the deadline — for any problems contact D. Paul, as above.

Technical specifications of the Beamline and instrumentation available are described in the *XMaS* web page.

When preparing your application, please consider the following:

- All sections of the form must be filled in. Particular attention should be given to the safety aspects, and the name and characteristics of the substance completed carefully. Experimental conditions requiring special safety precautions such as the use of lasers, high pressure cells, dangerous substances, toxic substances

and radioactive materials, must be clearly stated in the proposal. Moreover, any ancillary equipment supplied by the user must conform with the appropriate French regulations. Further information may be obtained from the ESRF Experimental Safety Officer, tel: +33 (0)4 76 88 23 69; fax: +33 (0)4 76 88 24 18.

- Please indicate your date preferences, including any dates that you would be unable to attend if invited for an experiment. This will help us to produce a schedule that is satisfactory for all.
- An experimental report on previous measurements must be submitted. New applications will not be considered unless a report on previous work is submitted. These also should be submitted electronically, following the ESRF model. The procedure for the submission follows that for the submission of proposals — again, follow the instructions in the ESRF’s web pages carefully. Reports must be submitted within 6 months of the experiment.
- The XMaS beamline is available for one third of its operational time to the ESRF’s user community. Applications for beamtime within that quota should be made in the ESRF’s proposal round - **Note: their deadlines are earlier than for XMaS! - 1st March and 1st September.** Applications for the same experiment may be made both to XMaS directly and to the ESRF. Obviously proposals successfully awarded beamtime by the ESRF will not then be given beamtime additionally in the XMaS allocation.

Assessment of Applications

The Peer Review Panel for the UK-CRG considers the proposals, grades them according to scientific excellence, adjusts the requested beam time if required, and recommends proposals to be allocated beam time on the beamline.

Proposals which are allocated beam time must in addition meet ESRF safety and XMaS technical feasibility requirements.

Following each meeting of the Peer Review Panel, proposers will be informed of the decisions taken and some feedback provided.



XMaS is an EPSRC sponsored project

